Ecological Indicators 181 (2025) 114382

Contents lists available at ScienceDirect

Ecological Indicators

journal homepage: www.elsevier.com/locate/ecolind

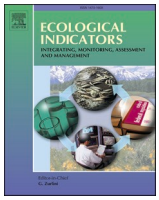

Original Articles

Spectral remote sensing reveals forest structural characteristics resilient to spruce budworm infestations

Tommaso Trotto [a,*], Nicholas C. Coops [a], Alexis Achim [b], Sarah E. Gergel [c]

[a] Department of Forest Resources Management, University of British Columbia, 2424 Main Mall, Vancouver, BC V6T 1Z4, Canada
[b] Département des sciences du bois et de la forêt, Université Laval, 2425 rue de la Terrasse, Québec, QC G1V 0A6, Canada
[c] Department of Forest and Conservation Sciences, Faculty of Forestry, University of British Columbia, 2424 Main Mall, Vancouver, BC V6T 1Z4, Canada

ARTICLE INFO

Keywords:
Time series
Landsat
Boreal forest
Clustering
Landscape disturbance
Impact assessment

ABSTRACT

Forests are increasingly influence by natural disturbance, which are intensifying under climate change, threatening the sustainability of natural resources. Resilience is a central component in these dynamics, defined as the ability of forests to recover from a disturbance and return to a pre-disturbed state. Recent conceptual frameworks describe resilience as a combination of disturbance impact and recovery rate offering a more unified and quantitative approach. However, these frameworks often do not consider how forest characteristics and their spatio-temporal variability shape resilience outcomes. In this study, we leveraged three decades of Landsat time series data to quantify forest resilience to spruce budworm (SBW) infestations, a major defoliator of fir and spruce forests in Quebec, Canada. We applied a two-stage clustering analysis to investigate how pre-disturbance forest structures, including canopy height, cover, basal area, cumulative defoliation severity, and age influence resilience. Resilience was quantified via impact and recovery rate of three key spectral indexes: Green Normalized Vegetation Index (GNDVI, greenness), Moisture Stress Index (MSI, vegetation water content), and Normalized Burn Ratio (NBR, structural characteristics) following the 2006 outbreak. Our results revealed that stands with lower basal area, sparser, and shorter canopies were more resilience to SBW over time. Greenness recovered most rapidly, followed by structural development and vegetation water content. Ultimately, stands showed greater resilient in greenness and structural development than vegetation water content throughout the infestation. These findings advance empirical understanding of forest resilience and can inform management strategies to maintain and enhance Canada's boreal forest resilience to increasing SBW pressure.

1. Introduction

Natural disturbances are primary drivers of forest dynamics and succession. Under a changing climate, historical disturbance regimes are being altered, intensifying their severity and spatial extent. These changes threaten the sustainability and health of natural resources (Trumbore et al., 2015), as disturbances can trigger gradual or abrupt landscape reorganization, potentially leading to alternative ecological states with novel species compositions and dynamics (Scheffer et al., 2001). Therefore, understanding how forests respond and adapt to disturbances is of paramount importance. However, forest responses to disturbances are often non-linear, scale-dependent, and influenced by stochasticity in disturbance events (Buma, 2015; Sturtevant & Fortin, 2021). These complexities make it difficult to predict whether disturbed forests will revert to their original structure and function or transition to alternative states. Therefore, a key challenge in forest management today is determining how to mitigate disturbance impacts and foster recovery. To investigate this, researchers have increasingly focused on how to maintain and enhance forest resistance and resilience to disturbances (Seidl et al., 2016; Standish et al., 2014).

Forest resistance can be defined as the ability of an ecological system to persist to an immediate disturbance, while resilience represents the ability of a system to recover from a disturbance and return to a pre-disturbed state ("engineering resilience") (Hodgson et al., 2015; Holling, 1973, 1996; Nimmo et al., 2015; Standish et al., 2014). Following this definition, a forest that has undergone a disturbance exhibits greater resistance if the disturbance has a lower impact, while greater resilience combines resistance with more rapid recovery. However, quantifying forest resistance and resilience to disturbances remains challenging, and those are often assessed through multiple components, including

* Corresponding author.
E-mail address: ttrotto@mail.ubc.ca (T. Trotto).

https://doi.org/10.1016/j.ecolind.2025.114382
Received 7 August 2025; Received in revised form 21 October 2025; Accepted 26 October 2025
Available online 8 November 2025

recovery rate and disturbance impact (Yi & Jackson, 2021). While these components contribute to resilience, recovery rate is frequently prioritized as the most direct indicator of resilience, as it reflects the capacity to rebound post-disturbances (Johnstone et al., 2016; Seidl et al., 2016). However, a forest with high recovery rate may still exhibit low resistance to disturbance (Hodgson et al., 2015). Thus, the most resilient forests are characterized primarily by lower initial impacts and secondarily by faster recovery rates (Hodgson et al., 2015; Nimmo et al., 2015).

Building on the recommendation of Hodgson et al. (2015) and Nimmo et al. (2015), Ingrisch & Bahn (2018) proposed a framework to estimate engineering resilience (Holling, 1996), which represents resilience as a combination of both impact and recovery rate from a disturbance, normalized to a baseline state for cross-study comparability. These two axes can be represented in a bivariate space. While this framework is novel as it offers a unified way to quantitatively estimate resilience based on both resistance and recovery (Scheffer et al., 2015), it remains largely conceptual. To operationalize it, further research is needed to identify the underlying mechanisms driving resilience to disturbances and to understand how their spatio-temporal variability influences resilience and its quantification, for example in landscapes affected by wildfires, insect outbreaks, and other disturbances.

In eastern Canada, landscape-level bioclimatic conditions drive the cyclical outbreaks of eastern spruce budworm (*Choristoneura fumiferana,* Clem, SBW), a native defoliator of spruce and fir forests (Candau and Fleming, 2005; Pureswaran et al., 2018b). SBW outbreaks typically recur every 30–40 years, affecting landscapes dominated by balsam fir (*Abies balsamea* L. (Mill.)), white spruce (*Picea glauca* (Moench) Voss), and black spruce (*Picea mariana* Mill.) under more severe infestations (Bognounou et al., 2017; Nealis & Régnière, 2004; Pothier et al., 2012). Recurring attacks have profound effects on forest health, for example resulting in delayed stand-level mortality, limited photosynthetic capacity (Candau & Fleming, 2005; Navarro et al., 2018), reduction in height and canopy cover (Trotto et al., 2024), potentially increased carbon emissions (Gunn et al., 2020), as well as diverse effects on post-disturbance recovery (Bouchard et al., 2006; Spence & MacLean, 2012). Furthermore, recent studies have suggested that increased fragmentation of host species stands may increase infestation risk and unpredictability (McNie et al., 2023, 2024; Trotto et al., 2025), while other research has instead shown that mixed species stands may reduce infestation severity (Zhang et al., 2018, 2020). Therefore, it is a priority to understand the potential implications of SBW infestations on forest resilience and investigate which forest attributes and their spatio-temporal variability modulate these responses. Doing so will help bridge the gap between conceptual frameworks and their practical application in forest management.

However, quantifying the effect of specific forest characteristics and their spatio-temporal variability on forest resistance and resilience to SBW presents significant challenges. SBW is highly mobile, and climatic changes may promote attacks through northward range expansion (Régnière et al., 2012), local adaptations to colder environments (Butterson et al., 2021), improved phenological synchronism between budburst and larval emergence (Pureswaran et al., 2018a), and potentially more severe and prolonged infestations (Bellemin-Noël et al., 2021; Gray, 2008, 2013; Subedi et al., 2023). These factors introduce complex, multi-scale variability in forest resistance and resilience mechanisms. Sánchez-Pinillos et al. (2019) addressed this challenge by analyzing changes in forest structure and composition to estimate plot-level resistance and resilience to SBW infestation in southern Quebec. In addition, the authors used pathway analysis to track post-disturbance trajectories of forest conditions for each plot relative to a pre-disturbance state and determine the direction and magnitude of the change in forest conditions. Their findings revealed species-specific responses, with pure balsam fir populations exhibiting lower resistance and resilience than secondary host species like black spruce. Moreover, infestation severity emerged as one of the most important drivers of these dynamics. However, this analysis was restricted to plot observations, which constrains the ability to capture how the spatio-temporal variability in forest attributes affects resistance and recovery responses to infestations, which is crucial when considering the large habitat range of SBW populations.

To address this gap, remote sensing imagery provides a unique opportunity to monitor forest responses to insect disturbances and their spatio-temporal variability, especially from long-term satellite missions (Rhodes et al., 2022; Senf et al., 2017; Wulder et al., 2022). In particular, spectral indexes derived from optical remote sensing have been previously adopted to successfully characterize the presence of SBW infestations on the landscape (Donovan et al., 2021), and have been utilized to detect regime shifts and changes in resilience in wetlands (Martinez et al., 2024). In their study, Martinez et al. (2024) reported on the usefulness of Normalized Difference Vegetation Index (NDVI), derived from Landsat, as early warning indicators of ecological transitions from forest to marsh environments. Their findings highlight the potential to employ spectral indexes to investigate resilience dynamics. Similarly, spectral indexes capturing forest structural and vegetation physiological characteristics have been widely employed to investigate recovery dynamics in complex ecosystems across Canada (Pickell et al., 2016; White et al., 2017, 2022). Landsat spectral composites have also been proven particularly valuable for characterizing and tracking forest attributes and disturbances with a level of detail relevant for forest inventory purposes and operational forest management (Brosofske et al., 2014; Hermosilla et al., 2015; White et al., 2014; Woodcock et al., 1994; Wulder et al., 2022). In parallel, the increasing availability of airborne laser scanning (ALS) data has significantly enhanced our capacity to characterize forest structure, complementing traditional spectral imagery (Wulder et al., 2012). While ALS acquisitions remain limited in spatial cover and temporal frequency compared to optical data, well-established approaches have facilitated the extrapolation of ALS-derived structural attributes beyond direct ALS coverage (Coops et al., 2021). Notably, imputed structural layers combining Landsat surface reflectance composites (White et al., 2014) with environment descriptors (e.g. topography) have generated wall-to-wall estimates of canopy height, cover, aboveground biomass, stem volume, and more across Canada's boreal forest since 1984 (Matasci et al., 2018).

Capitalizing on the availability of long time series data of forest conditions, structural layers, and disturbance dynamics, this study investigates what pre-infestation structural forest attributes and their spatio-temporal variability led to greater resilience to SBW infestations in the eastern boreal forests of Quebec, Canada, since the beginning of the most recent outbreak in 2006. In doing so, we apply the framework of Ingrisch & Bahn (2018) to estimate forest resilience to SBW infestations as a function of infestation impact and post-disturbance recovery rate derived from Landsat surface reflectance time series data. In particular, we address two key questions. First, can spectral indexes derived from Landsat surface reflectance composites capture resilience patterns to SBW infestations? Secondly, what forest structural attributes, imputed from Landsat, are mostly involved in resilience mechanisms to SBW infestations?

2. Study area and data

2.1. Study area description

We focus on the closed-canopy boreal forest sub-ecozone of Quebec, Canada, extending over approximately 50 Mha between 48°N and 52°N latitude. This sub-ecozone is part of the boreal ecozone of Quebec and encompasses two bioclimatic domains. The Spruce – Feathermoss domain is dominated by a mixture of balsam fir and black spruce in the north, forming denser forests with closed canopies, and the Balsam Fir – White Birch (Betula papyrifera Marshall) in the southern part, characterized by larger balsam fir populations, intermixed with deciduous forest further south. Furthermore, the sub-ecozone is classified into four

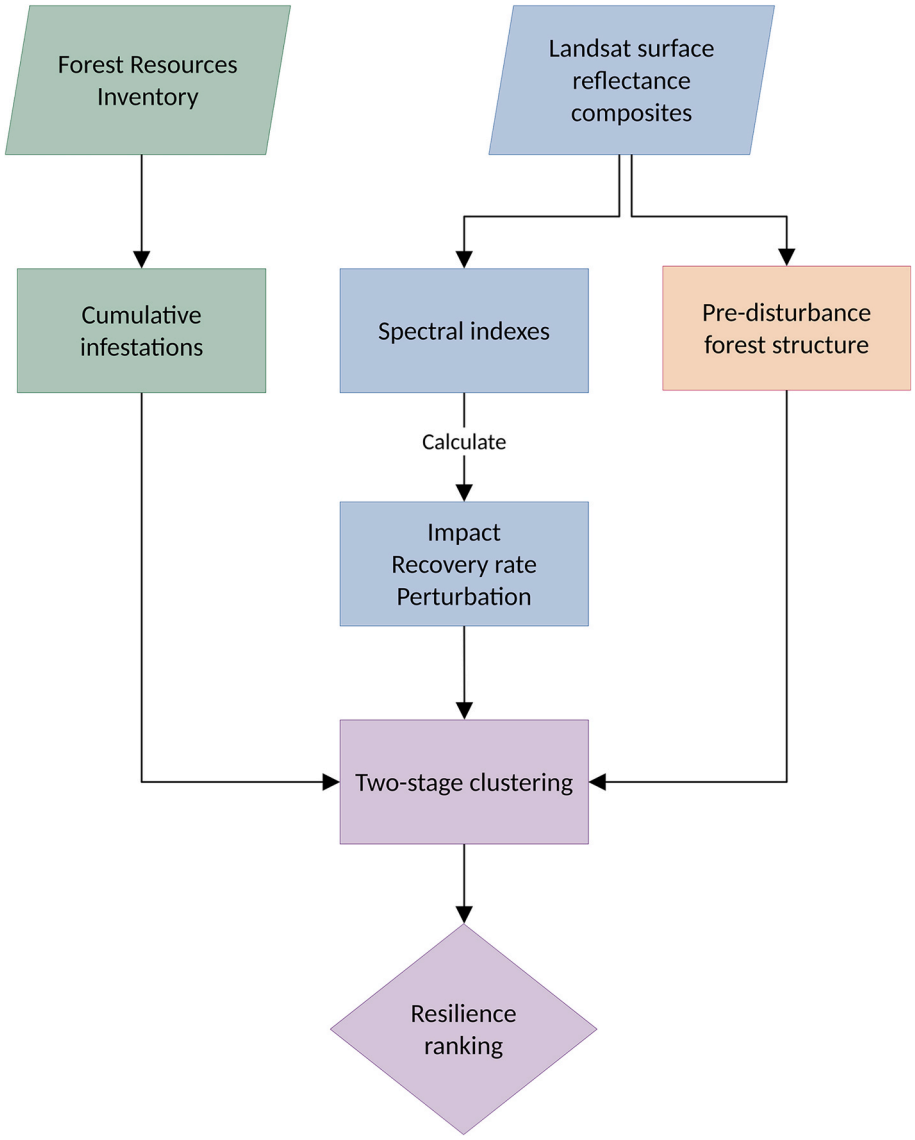

Fig. 1. Illustration of the workflow adopted in this research. Consistent colors were used to indicate logical connections between related workflow stages.

sub-domains: the northern east–west Spruce – Feathermoss sub-domains (SF-E, SF-W), and the southern east–west Balsam Fir – White Birch sub-domains (BW-E, BW-W). Land cover type for the sub-ecozone is predominantly coniferous (24 Mha – 47.5 %), followed by mixedwood forests (7.4 Mha – 14.8 %) and deciduous (1 Mha – 2 %) as of 2022 (Hermosilla et al., 2022). In this research, we focused on the SF-E, BW-E, and BW-W areas, where most of the infestations occurred, and in particular, only in conifer-dominated land covers, which covered approximately 13 Mha.

Historical climate normals for the period 1991–2020 show mean annual precipitation ranging between 702 and 1417 mm and mean annual temperature between −4.1 and 3.8 °C across the study area (Figs. S1A-B) (Wang et al., 2016). The elevation of the area ranged from 23 – 846 m (Fig. S1C) as derived from the Advanced Spaceborne Thermal Emission and Reflection Radiometer (ASTER) Global Digital Elevation Model v3 (Abrams et al., 2022).

2.2. Data sources

In this analysis, we capitalized on three key datasets. First, we downloaded annual forest health sketch maps from the Forest Resources Inventory (FRI) from the Quebec Ministère des Ressources naturelles et des Forêts between 2006 and 2022. These maps are produced by trained professionals during regular aerial overview surveys (AOS) assessments in the region. The year 2006 was selected as the first year of the last outbreak based on the forest health maps. Secondly, we acquired Landsat best available surface reflectance composites (BAP) at annual time steps for the last 31 years (1991 – 2022) available from the National Terrestrial Ecosystem Monitoring System (NTEMS) (White et al., 2014) at 30 m spatial resolution. The year 1991 was selected as the year marking the end of the previous outbreak, which occurred approximately between 1970 and 1990 in the study area according to the forest health maps. Thirdly, we acquired pre-disturbance structural layers from NTEMS at the beginning of the last outbreak in 2006. While AOS provide broad-scale information on SBW infestations and other disturbances, BAP composites offer greater spatial resolution and geometric accuracy for spatially-explicit, temporal analysis of forest dynamics.

2.3. Landsat surface reflectance composites and pre-disturbance structural layers

Surface reflectance composites were derived from Landsat time series via the Composite2Change (C2C) approach (Hermosilla et al., 2016) distributed as part of NTEMS data products. We downloaded layers

between 1991 and 2022. The C2C approach produces gap-free surface reflectance composites at annual time steps at a 30 m resolution (Hermosilla et al., 2016). We included land cover information derived from the Virtual Land Cover Engine (Hermosilla et al., 2022), as well as disturbance information related to the occurrence of wildfire and harvesting to isolate the effect of SBW infestations on the landscape. In addition, to understand pre-disturbance forest structural responses to SBW infestations, we utilized forest structural layers imputed from BAP surface composites (Matasci et al., 2018) which included canopy cover, height, and basal area, as well as forest age (Maltman et al., 2023) (Figs. S2). Prior to use the forest structural layers, we screened for outliers by retaining the 5 – 95 interquartile range of the data.

2.4. Forest resources inventory

Forest health maps were acquired between 2006 and 2022 from the Quebec Ministère des Ressources naturelles et des Forêts. These are conducted annually, where trained professionals delineate regions of current defoliation, classified into three severity classes (light, moderate, severe) as a function of the amount of tree infested and the proportion of the crown defoliated (Ministère des Ressources Naturelles et des Forêts, 2024a). Light infestations represent a loss of foliage in the upper third canopy of a few trees. Moderate infestations represent a loss of foliage in the upper half canopy of most trees. Severe infestations represent a loss of foliage across the entire crown length of most trees. Further, we acquired vector layers mapping roads and water bodies, as well as wildfires and harvesting operations since 1991 at a minimum mapping unit (MMU) of 0.1 ha for masking purposes.

3. Methods

The overarching methodological steps applied in this research are summarized in Fig. 1 and explained in details in the following sections.

3.1. Disturbance mapping

We compiled a cumulative disturbance map for SBW infestations from the AOS for each year by rasterizing vector layers at 30 m to match the resolution of the Landsat products. To do so, we assigned an increasing integer value to moderate and severe classes only (moderate: 2, severe: 3), then summed them over time. Light infestations were not included in the analysis as these may carry greater accuracy errors and detectability than higher severity classes (Donovan et al., 2021; Thompson et al., 2007). To isolate the presence of SBW on the landscape, a mask was produced by combining FRI information on wildfires, harvesting, roads, and water bodies between 1991 and 2022 with a 30 m buffer. We also removed young, short stands with low basal area as these are typically not the primary host of SBW (Blais, 1958; MacLean, 1980; Virgin & MacLean, 2017). To do so, we used canopy cover and height structural layers, as well as forest age to remove stands with < 25 % of canopy cover (Trotto et al., 2024), less than 7 m in height according to the inventory standard of the Quebec Ministry (Ministère des Ressources Naturelles et des Forêts, 2024b), and younger than 20 years of age based on the age class distribution used in the regular inventory cycles (Ministère des Ressources Naturelles et des Forêts, 2024b). Finally, to avoid including pixels that exhibited high impact and low recovery rate due to unrelated land cover changes, we selected only infested pixels in areas consistently classified as coniferous forest cover from 1991 to 2022, as per NTEMS, which represented approximately 85 % of the total infested pixels. Undisturbed areas represented non-masked coniferous land cover pixels that did not experience any disturbance from 15 years prior to the first year of the last infestation in 2006 and throughout the analysis period, post-disturbance to 2022. Areas meeting these selection criteria were mainly located in the northern part of the study area and covered approximately 3 Mha.

Outbreaks typically result in recurrent infestations across multiple years. To isolate post-infestation recovery rate, we first selected pixels that had an infestation starting in 2006. We then tracked the annual infestation severity of these pixels through time to 2022. We subset only stands where the infestation stopped at some point post 2006 and the stands remained infestation-free for another five years. As a result, the infestation length and cumulative severity will change on a pixel basis, yet all selected stands will have had at least five infestation-free years up to 2022. Most of the selected pixels were within the last seven years of the time series, corresponding with a decline of the SBW outbreak, which allowed previously-infested stands to recover. Finally, for each selected pixel we extracted the corresponding spectral values from the BAP composites.

Table 1
Definition of selected spectral indexes. B – blue, G – green, R – red, NIR – near infrared, SWIR1 – shortwave infrared 1, SWIR2 – shortwave infrared 2. These indexes were used to quantify forest resilience to SBW infestations in greenness, vegetation water content, and structural development.

Index/ Process	Description	Equation	Rationale	Reference
Greenness				
GNDVI	Green Normalized Difference Vegetation Index	$\frac{(NIR\text{-}G)}{(NIR+G)}$	Changes in greenness are a direct and early indicator of infestations, and are easily detectable via remote sensing	Gitelson et al. (1996)
Vegetation water content				
MSI	Moisture Stress Index	$SWIR1/NIR$	Foliage loss and post-disturbance regrowth affect water content and MSI captures physiological stress responses to infestation	Hunt & Rock (1989)
Structure				
NBR	Normalized Burn Ratio	$\frac{(NIR\text{-}SWIR2)}{(NIR+SWIR2)}$	Structural changes occur gradually, but are key to informing forest management decisions	Key & Benson (2006)

Table 2
Definition of impact, recovery rate, and perturbation used in the bivariate framework to estimate forest resilience to SBW infestations from spectral information. 'S' is the spectral index value at time of impact 't_i' (e.g. 2017) and 'B' is the baseline level.

Definition	Equation	Reference
Spectral impact of moderate or severe infestations	$Impact = (S_{2006}\text{-}S_{ti})/B$	Modified from Ingrisch & Bahn (2018)
Spectral recovery rate over a 5-year period from moderate or severe infestations	$Recovery\ rate = (S_{ti+5}\text{-}S_{ti})/5/B$	Ingrisch & Bahn (2018)
Cumulative reduction of spectral value as a function of impact and recovery rate	$Perturbation = \frac{Impact^2}{2 \cdot Recovery\ rate}$	Ingrisch & Bahn (2018)

3.2. Quantifying resilience

We calculated three spectral indexes (Table 1) that have been shown to be useful to characterize the presence of SBW infestation on the landscape (Donovan et al., 2021) and used them to quantify resilience. Each index targets a specific physiological process: canopy chlorophyll content, foliage moisture, and stand structure. These indexes were used

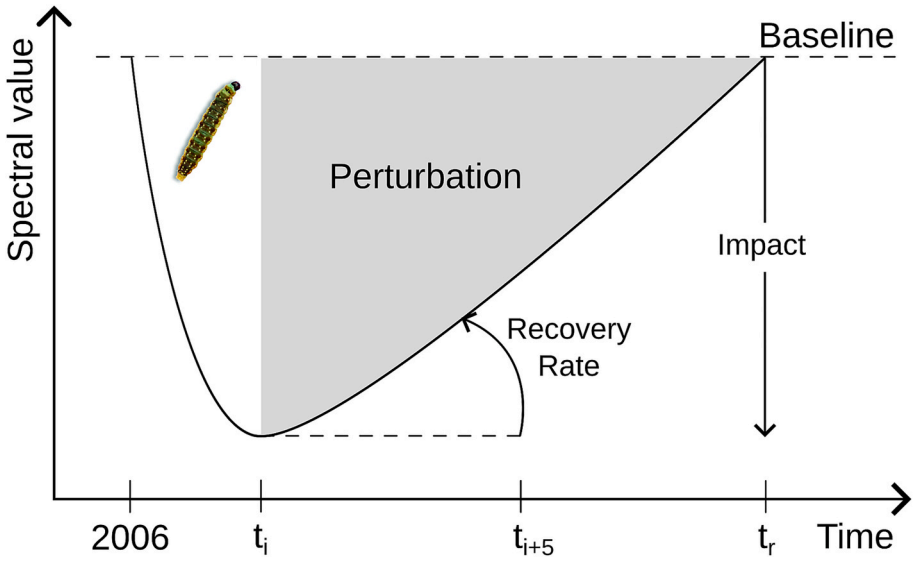

Fig. 2. Conceptual diagram illustrating how impact, recovery rate, and perturbation are quantified based on spectral values. Adapted from Ingrisch & Bahn (2018). SBW image obtained from Natural Resource Canada, licensed under the Open Government Licence – Canada, at https://natural-resources.canada.ca/forest-forestry/insects-disturbances/spruce-budworm.

Table 3
List of input variable in the two-stage clustering to quantify resilience to SBW infestations. 'S' is the spectral index value at time of impact 't_i' (e.g. 2017) and 'B' is the baseline level.

Feature	Definition	Reference
Impact	$(S_{2006}\text{-}S_{ti})/B$	Modified from Ingrisch & Bahn (2018)
Recovery rate	$(S_{ti+5}\text{-}S_{ti})/5/B$	Ingrisch & Bahn (2018)
Perturbation	$\frac{Impact^2}{2 \cdot Recovery\ rate}$	Ingrisch & Bahn (2018)
Pre-disturbance height (m)	95th percentile of first returns height	Matasci et al. (2018)
Pre-disturbance canopy cover (%)	Proportion of first returns above 2 m	Matasci et al. (2018)
Pre-disturbance basal area (m^2/ha)	Cross-sectional area of tree stems at 1.3 m per hectare	Matasci et al. (2018)
Pre-disturbance age	Age in 2006	Maltman et al. (2023)
Cumulative infestation	Cumulative infestation from annual disturbance layers at year of impact	This study

to examine how resilience varies across these different physiological dimensions. The normalized burn ratio (NBR, Key & Benson (2006)), capturing forest structural development, was also included as it is commonly used to detect changes in spectral trajectories associated with forest disturbances (Hermosilla et al., 2015).

To estimate forest resilience to SBW infestations, we followed Ingrisch & Bahn (2018). First, we estimated a baseline level for each spectral index, defined as the median spectral index value for undisturbed forested pixels. We then estimated infestation impact and recovery rate for each index (Table 2). To do so, we calculated the infestation impact in each pixel as the reduction in the index from the pre-disturbance conditions to the last year of infestation before recovery. We then calculated the recovery rate as the slope of the return in the spectral index from the last year of infestation to the end of five post-disturbance years. Next, we used the baselines to normalize the impact and recovery rate for each index. Finally, we quantified the cumulative effect of infestation (hereafter "perturbation") by calculating the area under the curve of the spectral index between the disturbed conditions and recovery, therefore integrating both the magnitude of impact and the recovery rate. This resulted in three metrics of resilience for each index: impact, recovery rate, and perturbation, each normalized by the baselines (Table 2, Fig. 2) (Ingrisch & Bahn, 2018).

3.3. Linking resilience responses to forest structure via clustering

To investigate which pre-disturbance forest structural conditions were associated with changing responses to resilience, we conducted a series of clustering analyses separately for each spectral index (hereafter "resilience clusters"). To do so, for each spectral index, we built a dataset containing pre-disturbance structural information, cumulative infestations up to the last year of impact, and the calculated impact, recovery rate, and perturbation metrics. This resulted in a total of 8 features for each of the spectral indexes (Table 3). Next, we applied an initial k-means partitioning (Lloyd, 1982; MacQueen, 1967) using 10 pre-clusters, followed by multivariate agglomerative clustering (Murtagh & Contreras, 2012), which is commonly used for ecological regionalization representations (Coops et al., 2009, 2020; Guo et al., 2017; Hargrove & Hoffman, 2004; Snelder et al., 2010; Trotto et al., 2024). Prior to clustering, each input feature was scaled to the 5 – 95 interquartile range, centered to the median, and forced to unit variance. Multivariate noise was removed using a PCA (Jollifee, 2002) with three components. This was done by removing pixels whose any of three principal components was greater than the 5 – 95 interquartile range of the transformed data.

The k-means pass consisted of 1000 initialization steps using a k-means++ initializer (Arthur & Vassilvitskii, 2006) based on the Manhattan distance (Aggarwal et al., 2001), while the agglomerative clustering approach used a Ward's linkage function (Ward, 1963) and an arbitrary 25% scaled Manhattan distance cut-off threshold. Separability in the final clustering result was assessed on a subset of 10,000 pixels per cluster using a non-parametric Kruskal-Wallis rank sum test (Acar & Sun, 2013) and a two-sided Dunn's post-hoc multiple pairwise comparison test (Dunn, 1964) with a Sidak correction to control for errors associated with multiple comparisons (Šidák, 1967).

Cluster ranking was determined based on the disturbance impact, recovery rate, and perturbation of each cluster. To do so, we examined the bivariate space of impact and recovery rate for each index. First, we determined the resilience target in the bivariate space that had the lowest impact and greatest recovery rate, thus having the maximum

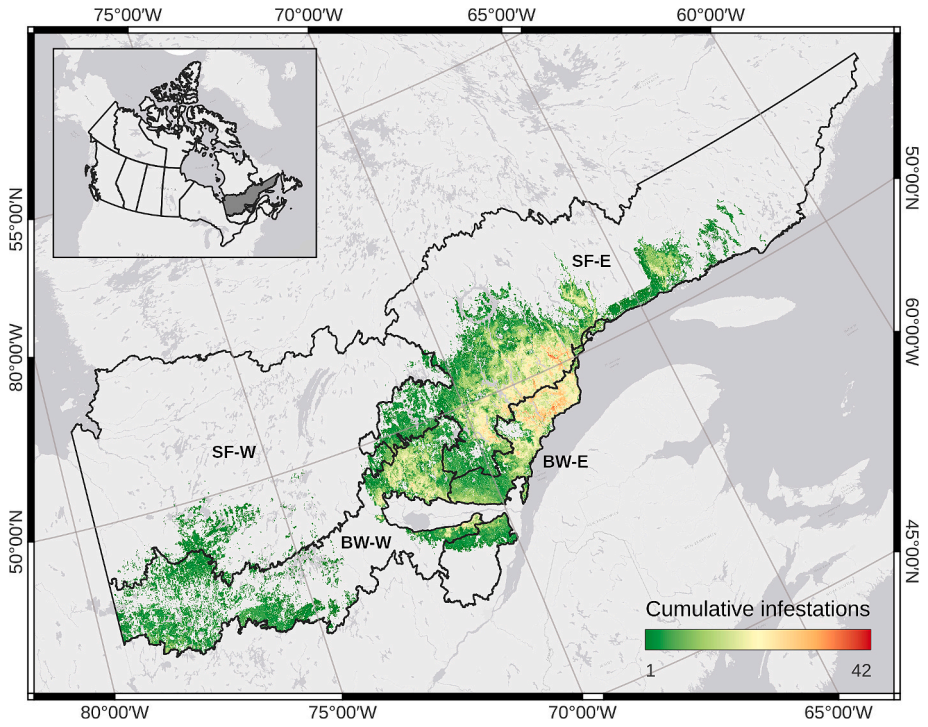

Fig. 3. Map of the study region showing the four sub-domains as classified by the Ministère des Ressources Naturelles et des Forêts of Quebec and the distribution of cumulative SBW infestation severity. SF: Spruce – Feathermoss; BF: Balsam Fir – White Birch; E: East; W: West.

resilience (Hodgson et al., 2015; Ingrisch & Bahn, 2018; Nimmo et al., 2015). We then calculated the Euclidean distance from that point to each cluster centroid, weighted by their corresponding amount of perturbation. Clusters further away from that point of maximum resilience indicate clusters with higher impact, lower recovery rate, and higher amount of perturbation and were therefore ranked lower in resilience.

4. Results

Since 2006, cumulative moderate and severe SBW infestations had covered a total of approximately 6.5 Mha (13% of the study area) (Fig. 3), characterized by an annual northward movement of the infestations until 2020, when the outbreak started to decline. Peaked infestations were observed between 2014 and 2016.

4.1. Assessment of resilience cluster separability

The two-stage clustering resulted in six final clusters. Clusters were ranked from 1 to 6, with cluster 1 being the most resilient and cluster 6 the least resilient. The results of the Kruskal-Wallis test applied to 10,000 samples for each index showed that the clusters were statistically well differentiated in spectral and structural features (p-value < 0.05). We then tested a total of 360 pairwise comparisons among clusters for each spectral and structural feature based on Dunn's post-hoc test, of which 17 (5%) were non-statistically significant and pertained to structural attributes. Overall, clusters 1 and 2 emerged as the most distinct clusters despite having similar cumulative infestations. Clusters 3 and 6 had similar pre-disturbance basal area and age. Clusters 3 – 4, and 5 – 6 had similar pre-disturbance tree height. Clusters 5 and 6 also had similar pre-disturbance basal area and cumulative infestations. Notably, the results of the Kruskal-Wallis test differed depending on the spectral index. In particular, clusters were better differentiated in terms

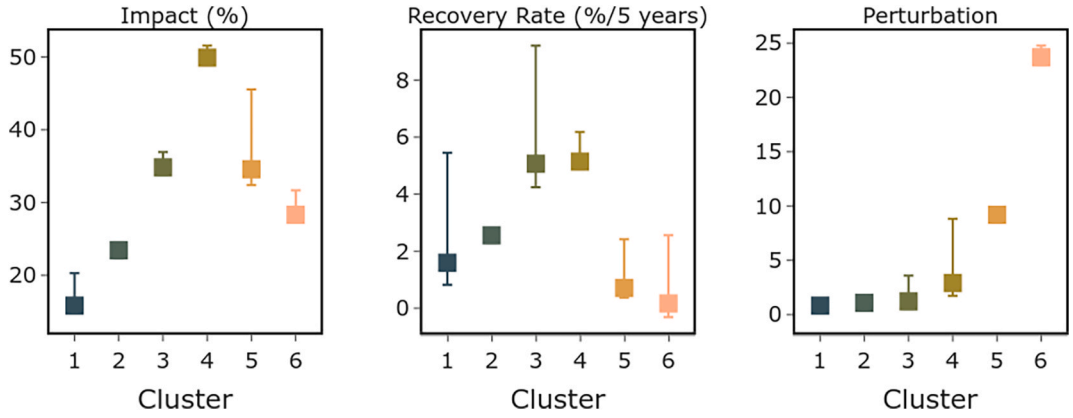

Fig. 4. Median impact, recovery rate, and perturbation across all spectral indexes. Impact is the percentage of change from pre-disturbance spectral values, recovery rate is the 5-year percentage increment in spectral value since the year of impact, and perturbation is a product of impact and recovery rate. Clusters are ranked from 1 to 6 based on decreasing resilience.

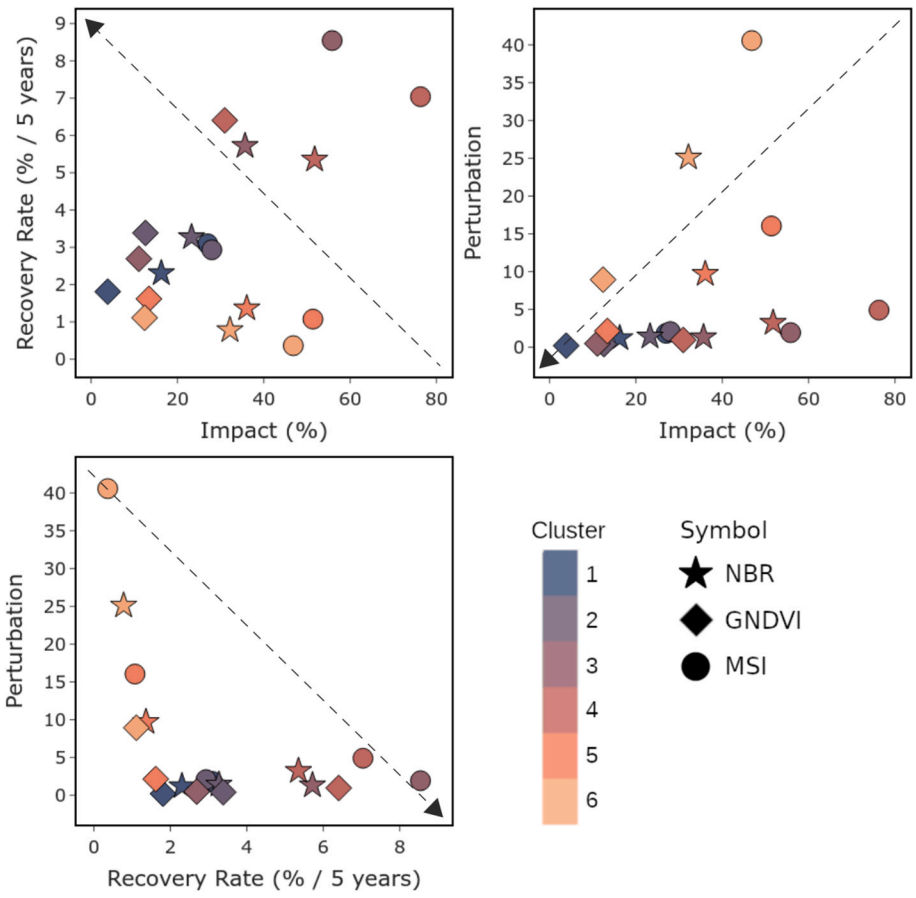

Fig. 5. Relations between impact, recovery rate, and perturbation for the six cluster centroids. Clusters are ranked 1 – 6 in decreasing order of resilience. Colors indicate the cluster rank, symbols indicate the spectral indexes, and the dashed arrows indicates the direction of increasing resilience.

of spectral and structural characteristics for NBR compared to the other indexes. Conversely, we found that GNDVI showed the most confusion among clusters for spectral and structural features.

4.2. Spectral impact, recovery rate, and perturbation responses

Results show that cluster 1 was the most resilient over time, characterized by the lowest impact and perturbation, and lower recovery rates than other clusters (Fig. 4). Cluster 2 was the second most resilient cluster, with a higher impact, recovery rate, and perturbation than cluster 1. Cluster 3 had the second highest impact and recovery rate and was characterized by a low perturbation. Cluster 4 was associated with the greatest impact and recovery rate of all clusters, and had a low perturbation, similar to clusters 1 – 3. Cluster 5 was the second lowest resilient cluster, with a lower impact than clusters 3 and 4 and a low recovery rate, and was associated with the second highest perturbation. Cluster 6 was the least resilient cluster, characterized by the lowest recovery rate and the greatest perturbation.

We examined the effect of infestations on each index separately (Fig. 5), and found that greenness in general exhibited lower impact, lower perturbation, and fast recovery rates over time, indicating greater resilience in greenness than moisture or structure. Moisture showed the most variable resilience responses of all spectral indexes and was associated with a greater impact than greenness or structure, suggesting lower resilience in moisture. Structure typically recovered more slowly than greenness but faster than moisture, and it exhibited greater impact than greenness but lower than moisture. Overall, structure demonstrated intermediate levels of resilience between greenness and moisture.

4.3. Structural characterization of the clusters

We observed that distinct pre-disturbance structural patterns emerged for each cluster across all indexes. In general, we found that cluster 1 had the lowest pre-disturbance canopy height, cover, basal area, and cumulative infestations (Fig. 6). Cluster 2 had the highest pre-disturbance canopy height, cover, and basal area (Fig. 6A–C), but showed low cumulative infestations similar to cluster 1 (Fig. 6E). Cluster 3 was associated with the second lowest pre-disturbance canopy height, cover, and basal area (Fig. 6A–C). Clusters 1 – 3 were older than clusters 4 – 6 and cluster 3 was the oldest (Fig. 6D). Cluster 4 and 5 were characterized by intermediate pre-disturbance canopy height (Fig. 6A), and were associated with the youngest stands (Fig. 6D) and the longest cumulative infestations (Fig. 6E). Cluster 5 also had the second highest pre-disturbance canopy cover and basal area (Fig. 6B and C) Cluster 6, the least resilient cluster to infestations, showed similar pre-disturbance structural characteristics to cluster 5, although was associated with older stands (Fig. 6D).

In addition, we examined the structural characteristics of the clusters for each index separately (Fig. 7). Overall, greenness, moisture, and structure showed resilience responses that matched the general structural characterization. However, greenness responses were more variable for clusters 2, 3, and 4, especially regarding pre-disturbance canopy height, cover, and cumulative infestations.

4.4. Clustering variability and its components

We examined the variance in the clustering using a PCA (Fig. 8). We found that spectral impact (68%) and pre-disturbance canopy cover (21%) explained 89% of the variance in greenness, followed by

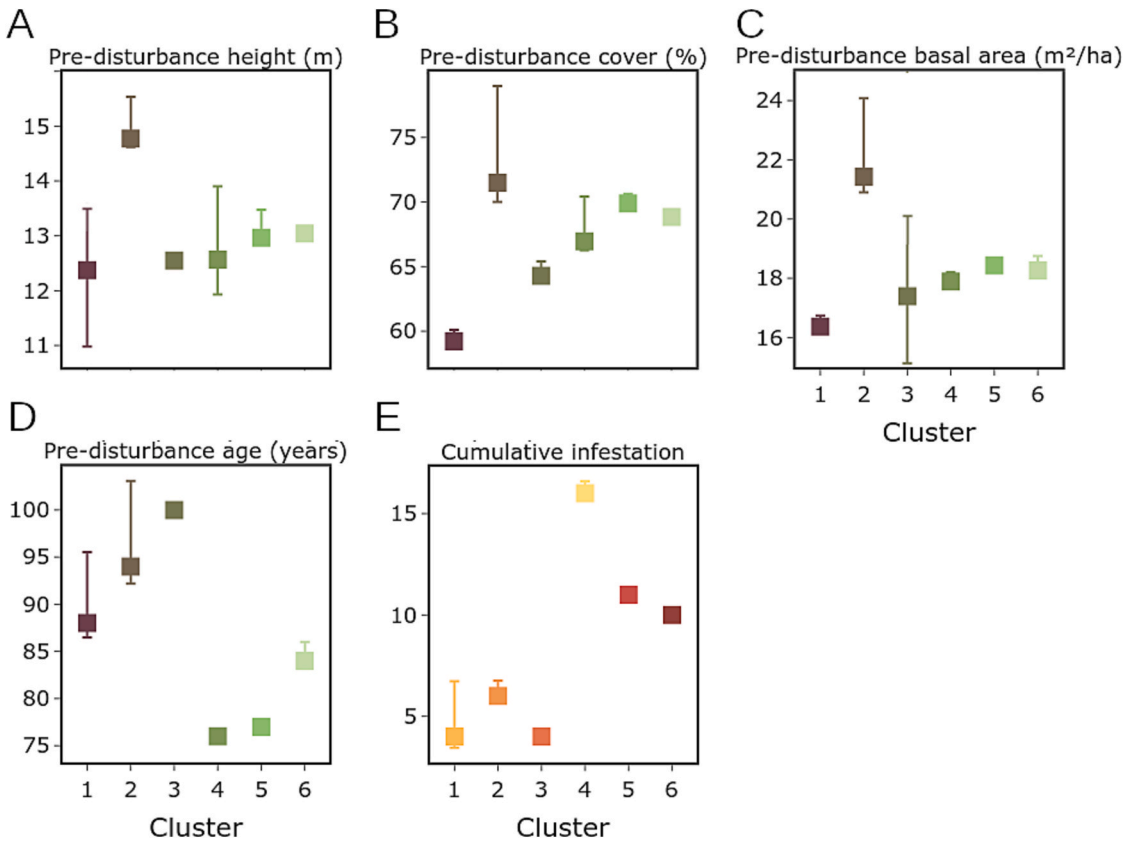

Fig. 6. Median pre-disturbance structural characteristics across all spectral indexes. Clusters are ranked from 1 to 6 based on decreasing resilience. To facilitate interpretation, two color palettes were used to differentiate structural characteristics (pre-disturbance height, cover, basal area, age) and cumulative infestations.

cumulative infestations (5%). Variance in moisture was also explained by spectral impact (49%) and canopy cover (31%), totally explaining 80% of the variance between the first two principal components, followed by cumulative infestations (14%). Similarly, variance in structural development was explained by spectral impact (60%) and canopy cover (20%), totally explaining 80% of the variance, followed by cumulative infestations (15%). Basal area and age explained smaller amounts of variance for each index (< 5%).

4.5. *Spatial distribution of clusters and resilience metrics*

The spatial distribution of the clusters varied by index (Fig. 9). Across the study area, clusters 1 and 2 were more spatially aggregated than other clusters for the structure-sensitive index NBR, and were primarily located closer to the epicenter of the outbreak. The epicenter of the infestation was located along the southern border of the BW-E subdomain, where the cumulative infestation was the highest for the analyzed period (Fig. 3). Conversely, clusters 3 – 6 were more dispersed. Clusters 1 and 2 were also spatially aggregated for the water-sensitive index MSI, although more interspersed with other clusters than NBR. Similar to NBR, clusters 3 – 6 were spatially dispersed. We also found that the greenness-sensitive index GNDVI was dominated by cluster 1, and we observed some spatial aggregation of clusters 2 and 3.

The spatial extent of the clusters also varied by index across the study area (Table 4). Cluster 1 was among the most represented across all indexes, extending between 35 – 77% of the total clustered area. The area covered by cluster 2 was also variable across indexes, covering between 6 – 44% of the total clustered area. An exception was GNDVI, where clusters 1 and 2 occupied 77% and 6% of the area, respectively. Overall, we found that the area occupied by cluster 3 was more consistent across indexes, ranging between 11 – 12%. Clusters 4 – 6 occupied a smaller extent compared to more resilient clusters 1 – 3. Cluster 4 occupied between 1 – 7% of the clustered area. Cluster 5 and 6 also extended over a small area, ranging between 1 – 3% across all indexes.

5. Discussion

Quantifying and monitoring resilience to disturbances remains challenging, and a deeper understanding of the forest structural characteristics and their spatio-temporal variability responsible for modulating forest resilience is needed to translate research into practice (Nikinmaa et al., 2020, 2024). In this research, we combined spectral and structural information from time series data to reveal forest spectral and structural responses to SBW infestations linked to resilience, in a spatially-explicit fashion. We identified response patterns that were consistently ranked as more resilient based on their impact, recovery rate, and amount of perturbation due to SBW infestations. Moreover, using a combination of spectral indexes was essential to capture the contribution of different physiological processes to resilience. Therefore, to effectively monitor and manage resilience to SBW infestations, future efforts should prioritize the use of complementary spectral indexes, for example that capture greenness, moisture, and structural changes.

5.1. *Remote sensing facilitates broad-scale resilience estimations*

We utilized Landsat time series to investigate patterns of forest resilience associated to SBW infestations in a spatially-explicit fashion. We found that the spatial aggregation of clusters varied by spectral index. In particular, spatial aggregations of clusters 1 and 2 were primarily found closer to the outbreak epicenter. This suggests that these clusters effectively showed greater resilience to infestations (lower impact and faster recovery) compared to lower resilience clusters. In addition, it is possible that the variability in species distribution

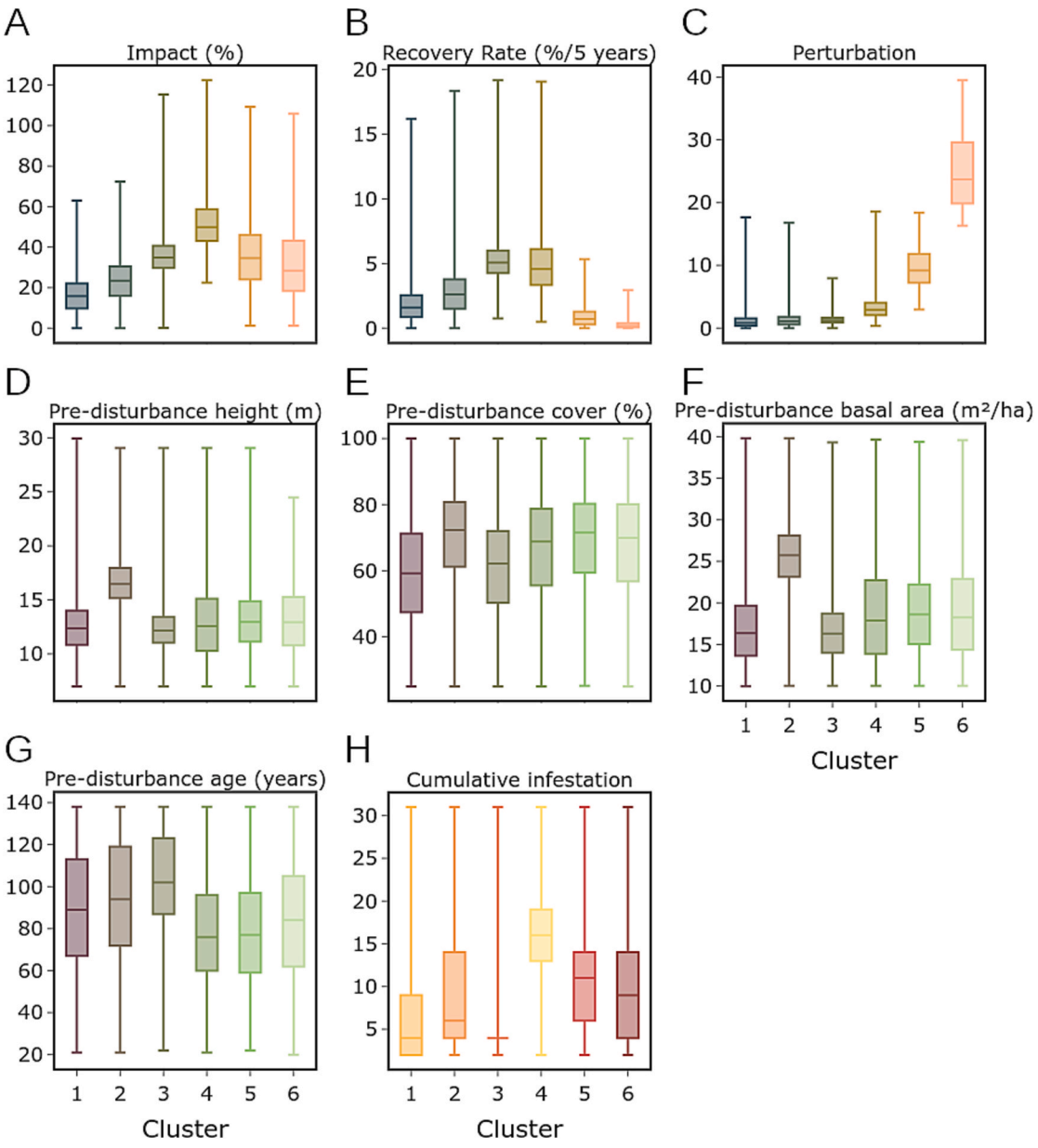

Fig. 7. Representative example of distribution of spectral and pre-disturbance structural characteristics for NBR. Clusters are ranked from 1 to 6 based on decreasing resilience. To facilitate interpretation, three color palettes were used to differentiate spectral (impact, recovery rate, perturbation) and structural characteristics (pre-disturbance height, cover, basal area, age) and cumulative infestations.

influenced the spatial distribution of the clusters. For instance, areas characterized by a greater proportion of host species may also suffer from greater infestation severity (Kneeshaw et al., 2021; Zhang et al., 2018, 2020), although this may depend on their spatial organization (McNie et al., 2023, 2024; Trotto et al., 2025).

The integration of diverse remote sensing products offers an opportunity to capture the spatio-temporal variability of key forest properties, such as structure and physiological processes, including foliage production and vegetation water content. However, it is essential to assess the complementarity of these data sources and determine which provides the most relevant insights. In our analysis, we used GNDVI to track changes in greenness and browning as infestations progressed across the landscape. This is important as infestations target foliage in the canopy and responses are readily observable from space (Donovan et al., 2021). MSI was included to assess vegetation water content, a known indicator for detecting and characterizing SBW infestations (Donovan et al., 2021), as it is directly linked to the presence of foliage in the canopy. In contrast, NBR was used to capture structural recovery following infestations.

5.2. *Diverse effects of post-infestation recovery associated with individual spectral indexes*

Our first objective was to investigate whether spectral indexes derived from Landsat surface reflectance composites can capture resilience patterns to SBW infestations, recognizing that post-disturbance recovery varies in timing and rates depending on the structural and functional attributes disturbed (Gatica-Saavedra et al., 2017; Trumbore et al., 2015; White et al., 2017, 2022). To do so, we used a set of spectral indexes describing different pre-disturbance forest physiological responses of greenness, moisture, and structural characteristics. We observed that impact and recovery in the greenness, captured by GNDVI, showed the lowest variability across all indexes, ranging between 4 – 30% in impact and 1.1 – 6.4% recovery rate over five years (Fig. 5). This

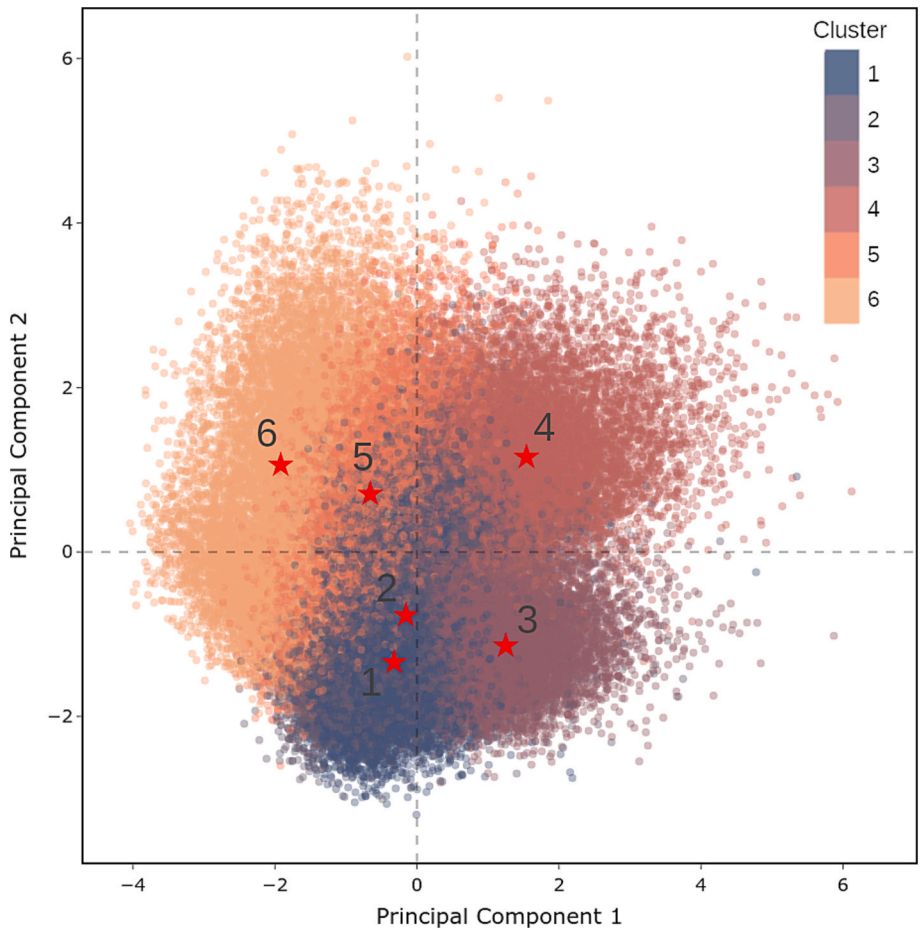

Fig. 8. Principal component space of spectral and pre-disturbance structural characteristics used in the NBR clustering showing the first two components based on a sample of 10,000 pixels per cluster. Red stars represent the centroids of each cluster, while colors represent the assigned resilience ranking. (For interpretation of the references to color in this figure legend, the reader is referred to the web version of this article.)

low variability likely reflects similar growth responses following infestations, which may accelerate greenness recovery as foliage amount and quality change post-infestations (De Grandpré et al., 2022; Piene & MacLean, 1999).

Water content in vegetation responded dynamically as the infestation progressed. Short-term effects on water content in vegetation have been observed to vary during and after defoliations (Bouzidi et al., 2019) as a result of vegetation recruitment and foliage development (Deslauriers et al., 2023). Consequently, we may expect water content in vegetation to recover at lower rates than foliage production. In our analysis, we observed variability in the recovery rates associated with vegetation water content (Fig. 5). In particular, MSI showed faster post-infestation recovery for clusters 3 and 4 than for lower resilience clusters.

Structural recovery, as indicated by NBR, is expected to occur after greenness recovery (Smith-Tripp et al., 2024), since understory and lateral growth help compensate for tree mortality. In our analysis, we found structural recovery rates were generally faster than those for vegetation water content, but lower than greenness recovery. The faster recovery rates we observed may be due to SBW attacks primarily targeting foliage, with limited mortality and thus causing short-term impacts on stand structure as affected trees redevelop their crown after the attack. Therefore, structural development is suggested to be more resilient than vegetation water content, which in turn depends on post-infestation foliage production.

5.3. Forest structural characteristics drive resilience responses to infestations

Our second objective was to identify what forest structural attributes, imputed from Landsat, are mostly involved in resilience mechanisms to SBW infestations. We found that stands with lower basal area, sparser, and shorter canopies exhibited the greatest resilience to SBW infestations over time. Stands characterized by a lower basal area (minimum tree height of 7 m) may promote larger and more vigorous crowns by releasing competition for light and resources (Bauce & Fuentealba, 2013; Gauthier et al., 2015; Power et al., 2024), resulting in potentially reduced vulnerability to attacks and a shorter recovery time to ongoing defoliations (Brookes, 1985; Colford-Gilks et al., 2012). Additionally,

moderate and severe infestations in lower basal area stands may potentially result in faster recovery rates than stands with higher initial basal area (Colford-Gilks et al., 2012). Consistent with this, we found that lower resilience clusters 4 – 6 were characterized by greater cumulative infestations on average and lower recovery rates than higher resilience clusters.

Pre-disturbance tree height explained a smaller amount of variance in the clusters, indicating that height may be less involved in forest resilience to infestations over time than other features such as basal area and canopy cover (Trotto et al., 2024). Notably, we found that tree height varied among high resilience clusters, with cluster 1 associated with the shortest and cluster 2 with the tallest canopies. This variability may reflect differences in tree height responses to the disturbance severity, for example by promoting tree height growth due to reduced

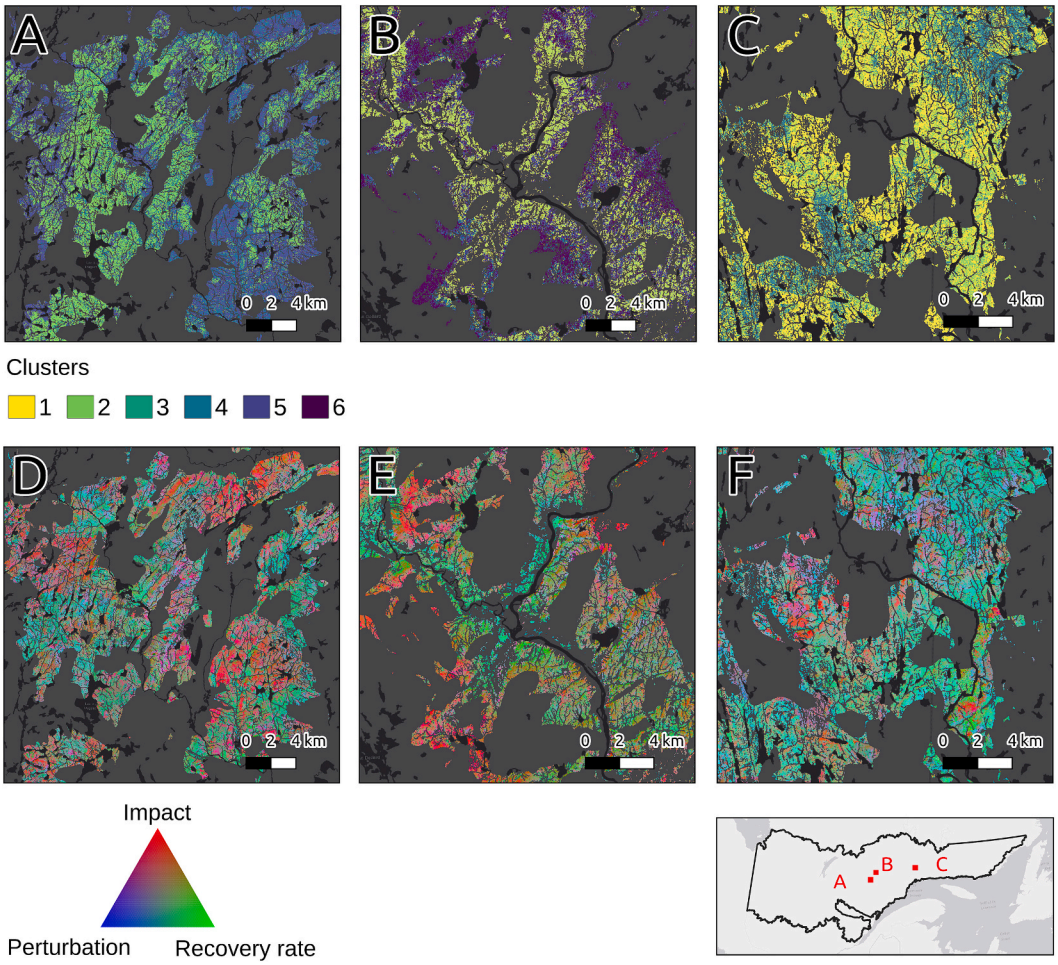

Fig. 9. View of three focus areas showing the distribution of (A – C) NBR clusters and (D – F) the corresponding impact, recovery rate, and perturbation values in 2017. At the bottom, red/purple shades are typically associated with higher impact and lower recovery rate (lower resilience), whereas green/cyan shades are typically associated with lower impact and higher recovery rate. (For interpretation of the references to color in this figure legend, the reader is referred to the web version of this article.)

Table 4
Summary of the percentage of clustered area covered by each cluster by spectral index.

Cluster	GNDVI – Greenness	MSI – Vegetation water content	NBR – Structure
Cluster 1	77	35	57
Cluster 2	6	44	20
Cluster 3	12	11	12
Cluster 4	1	7	7
Cluster 5	3	2	3
Cluster 6	1	1	1

competition, or facilitating increases in the complexity of the canopy cover over time (Choi et al., 2023; Trotto et al., 2024). Age responses also varied across resilience clusters. Mature stands, with a greater abundance of dominant and co-dominant balsam fir, may be more vulnerable to attacks than younger stands of intermediate host species strata (Blais, 1958). This may be due to mature stands showing larger, taller canopies that can host a larger SBW population, particularly during the early developmental stages (Blais, 1958). However, we found that all six clusters were associated with mature stands. Therefore, we would expect age responses to be linked with other structural characteristics, such as canopy cover and basal area. Thus, changes in canopy cover and basal area may have a greater effect on resilience to infestation over time than age alone.

5.4. Study limitations and inclusion of additional explanatory variables of resilience

We utilized a two-stage clustering approach to estimate resilience from spectral and structural forest attributes. However, capturing changes in spectral information associated to SBW infestations remains challenging. Candidate pixels for the analysis were selected from the AOS, which are known to have accuracy limitations (Thompson et al., 2007). Since AOS are designed to capture broad-scale patterns in forest health, aligning these data products with individual pixels may result in mixed spectral responses associated with SBW infestations. Additionally, we focused on temporally consistent land cover classes (Hermosilla et al., 2022) without incorporating individual species information, as these require more careful use (Hermosilla et al., 2024). However, by tracking stable coniferous land covers, we were able to identify broad-scale patterns of forest resilience to infestations using a combination of spectral and structural attributes in a more robust way. Climate data were not included in the research, as our objective was to isolate the influence of forest structure alone on resilience to SBW. Moreover,

Sánchez-Pinillos et al. (2019) did not find a statistically significant relationship between resilience to SBW infestations and temperature in their plot-level study conducted within the same bioclimatic domains. Nevertheless, future work should prioritize the inclusion of complementary variables to understand more complex abiotic and biotic interactions occurring at eco-regional scales as these can potentially influence resilience outcomes over time (Sánchez-Pinillos et al., 2019).

6. Conclusions

This study provides a spatially explicit assessment of forest resilience to SBW infestations using three decades of Landsat surface reflectance data. By quantifying the impact and recovery of key spectral indexes, we demonstrate that forest resilience is influenced by pre-disturbance structural attributes, including canopy cover, height, basal area, and age. Notably, stands characterized by lower basal area with sparser and shorter canopies exhibited greater resilience over time. Impact and recovery rates also varied by physiological process, with greater resilience observed in greenness, followed by structural development and vegetation water content. These findings underscore the importance of integrating forest structure and spectral information into resilience assessments and offer valuable insights for the development of management strategies aimed at enhancing the resilience of boreal forests under increasing SBW pressure.

CRediT authorship contribution statement

Tommaso Trotto: Writing – review & editing, Writing – original draft, Visualization, Software, Methodology, Investigation, Formal analysis, Conceptualization. **Nicholas C. Coops:** Writing – review & editing, Writing – original draft, Supervision, Resources, Methodology, Investigation, Funding acquisition, Conceptualization. **Alexis Achim:** Writing – review & editing, Funding acquisition, Conceptualization. **Sarah E. Gergel:** Writing – review & editing.

Funding

This research was funded by a NSERC Alliance project Silva21 NSERC ALLRP 556265–20, grantee Prof. Alexis Achim.

Declaration of competing interest

The authors declare that they have no known competing financial interests or personal relationships that could have appeared to influence the work reported in this paper.

Acknowledgements

This analysis was conducted at the University of British Columbia, which is located on the traditional, ancestral, and unceded land of the xʷməθkʷəy̓əm (Musqueam) people. We thank the anonymous reviewers whose feedback helped to improve and clarify this manuscript.

Appendix A. Supplementary data

Supplementary data to this article can be found online at https://doi.org/10.1016/j.ecolind.2025.114382.

Data availability

The FRI data is available from the Ministère des Ressources naturelles et des Forêts du Québec at https://www.donneesquebec.ca/recherche/dataset/donnees-sur-les-perturbations-naturelles-insecte-tordeuse-des-bourgeons-de-lepinette. The Landsat-derived products used in this paper are available at https://opendata.nfis.org/mapserver/nfis-change_eng.html. Digital elevation data from the ASTER satellite (version 3) is available at https://asterweb.jpl.nasa.gov/gdem.asp.

References

Abrams, M., Yamaguchi, Y., Crippen, R. (2022). ASTER GLOBAL DEM (GDEM) VERSION 3. The International Archives of the Photogrammetry, Remote Sensing and Spatial Information Sciences, XLIII-B4-2022, 593–598. XXIV ISPRS Congress “Imaging today, foreseeing tomorrow”, Commission IV -, 2022. edition, 6–11 June 2022. Nice, France. https://doi.org/10.5194/isprs-archives-XLIII-B4-2022-593-2022.

Acar, E.F., Sun, L., 2013. A Generalized Kruskal–Wallis Test Incorporating Group uncertainty with Application to Genetic Association Studies. Biometrics 69 (2), 427–435. https://doi.org/10.1111/biom.12006.

Aggarwal, C.C., Hinneburg, A., Keim, D.A., 2001. On the Surprising Behavior of Distance Metrics in High Dimensional Space. In: Van Den Bussche, J., Vianu, V. (Eds.), Database Theory—ICDT, 2001 (Vol. 1973. Springer, Berlin Heidelberg, pp. 420–434. https://doi.org/10.1007/3-540-44503-X_27.

Arthur, D., Vassilvitskii, S., 2006. k-means++: the Advantages of Careful Seeding. Stanford. http://ilpubs.stanford.edu:8090/778/.

Bauce, É., Fuentealba, A., 2013. Interactions between stand thinning, site quality and host tree species on spruce budworm biological performance and host tree resistance over a 6 year period after thinning. For. Ecol. Manage. 304, 212–223. https://doi.org/10.1016/j.foreco.2013.05.008.

Bellemin-Noël, B., Bourassa, S., Despland, E., De Grandpré, L., Pureswaran, D.S., 2021. Improved performance of the eastern spruce budworm on black spruce as warming temperatures disrupt phenological defences. Glob. Chang. Biol. 27 (14), 3358–3366. https://doi.org/10.1111/gcb.15643.

Blais, J.R., 1958. The vulnerability of balsam fir to spruce budworm attack in northwestern ontario, with special reference to the physiological age of the tree. For. Chron. 34 (4), 405–422. https://doi.org/10.5558/tfc34405-4.

Bognounou, F., De Grandpré, L., Pureswaran, D.S., Kneeshaw, D., 2017. Temporal variation in plant neighborhood effects on the defoliation of primary and secondary hosts by an insect pest. Ecosphere 8 (3), e01759. https://doi.org/10.1002/ecs2.1759.

Bouchard, M., Kneeshaw, D., Bergeron, Y., 2006. Forest dynamics after successive spruce budworm outbreaks in mixedwood forests. Ecology 87 (9), 2319–2329. https://doi.org/10.1890/0012-9658(2006)87%255B2319:FDASSB%255D2.0.CO;2.

Bouzidi, H.A., Balducci, L., Mackay, J., Deslauriers, A., 2019. Interactive effects of defoliation and water deficit on growth, water status, and mortality of black spruce (Picea mariana (Mill.) B.S.P.). Ann. For. Sci. 76 (1), 1. https://doi.org/10.1007/s13595-019-0809-z.

Brookes, M.H., 1985. *Managing Trees and Stands Susceptible to Western Spruce Budworm*. U. S, Forest Service, Cooperative State Research Service.

Brosofske, K.D., Froese, R.E., Falkowski, M.J., Banskota, A., 2014. A Review of Methods for Mapping and Prediction of Inventory Attributes for Operational Forest Management. For. Sci. 60 (4), 733–756. https://doi.org/10.5849/forsci.12-134.

Buma, B., 2015. Disturbance interactions: Characterization, prediction, and the potential for cascading effects. Ecosphere 6 (4), art70. https://doi.org/10.1890/ES15-00058.1.

Butterson, S., Roe, A.D., Marshall, K.E., 2021. Plasticity of cold hardiness in the eastern spruce budworm, *Choristoneura fumiferana*. Comp. Biochem. Physiol. A Mol. Integr. Physiol. 259, 110998. https://doi.org/10.1016/j.cbpa.2021.110998.

Candau, J.-N., Fleming, R.A., 2005. Landscape-scale spatial distribution of spruce budworm defoliation in relation to bioclimatic conditions. Can. J. For. Res. 35 (9), 2218–2232. https://doi.org/10.1139/x05-078.

Choi, D.H., LaRue, E.A., Atkins, J.W., Foster, J.R., Matthes, J.H., Fahey, R.T., Thapa, B., Fei, S., Hardiman, B.S., 2023. Short-term effects of moderate severity disturbances on forest canopy structure. J. Ecol. 111 (9), 1866–1881. https://doi.org/10.1111/1365-2745.14145.

Colford-Gilks, A.K., MacLean, D.A., Kershaw, J.A., Béland, M., 2012. Growth and mortality of balsam fir- and spruce-tolerant hardwood stands as influenced by stand characteristics and spruce budworm defoliation. For. Ecol. Manage. 280, 82–92. https://doi.org/10.1016/j.foreco.2012.05.023.

Coops, N.C., Shang, C., Wulder, M.A., White, J.C., Hermosilla, T., 2020. Change in forest condition: Characterizing non-stand replacing disturbances using time series satellite imagery. For. Ecol. Manage. 474, 118370. https://doi.org/10.1016/j.foreco.2020.118370.

Coops, N.C., Tompalski, P., Goodbody, T.R.H., Queinnec, M., Luther, J.E., Bolton, D.K., White, J.C., Wulder, M.A., Van Lier, O.R., Hermosilla, T., 2021. Modelling lidar-derived estimates of forest attributes over space and time: a review of approaches and future trends. Remote Sens. Environ. 260, 112477. https://doi.org/10.1016/j.rse.2021.112477.

Coops, N.C., Wulder, M.A., Iwanicka, D., 2009. An environmental domain classification of Canada using earth observation data for biodiversity assessment. Eco. Inform. 4 (1), 8–22. https://doi.org/10.1016/j.ecoinf.2008.09.005.

De Grandpré, L., Marchand, M., Kneeshaw, D.D., Paré, D., Boucher, D., Bourassa, S., Gervais, D., Simard, M., Griffin, J.M., Pureswaran, D.S., 2022. Defoliation-induced changes in foliage quality may trigger broad-scale insect outbreaks. Commun. Biol. 5 (1), 1–10. https://doi.org/10.1038/s42003-022-03407-8.

Deslauriers, A., Balducci, L., Fierravanti, A., Bouchard, M., 2023. Changes in Water Status and Carbon Allocation in Conifers Subjected to Spruce Budworm Defoliation and Consequences for tree Mortality and Forest Management. In: Girona, M.M., Morin, H., Gauthier, S., Bergeron, Y. (Eds.), *Boreal Forests in the Face of Climate Change: Sustainable Management*. Springer International Publishing, pp. 249–269. https://doi.org/10.1007/978-3-031-15988-6_9.

Donovan, S.D., MacLean, D.A., Zhang, Y., Lavigne, M.B., Kershaw, J.A., 2021. Evaluating annual spruce budworm defoliation using change detection of vegetation indices calculated from satellite hyperspectral imagery. Remote Sens. Environ. 253, 112204. https://doi.org/10.1016/j.rse.2020.112204.

Dunn, O.J., 1964. Multiple Comparisons using Rank Sums. Technometrics 6 (3), 241–252. https://doi.org/10.1080/00401706.1964.10490181.

Gatica-Saavedra, P., Echeverría, C., Nelson, C.R., 2017. Ecological indicators for assessing ecological success of forest restoration: a world review. Restor. Ecol. 25 (6), 850–857. https://doi.org/10.1111/rec.12586.

Gauthier, M.-M., Barrette, M., & Tremblay, S. (2015). Commercial Thinning to Meet Wood Production Objectives and Develop Structural Heterogeneity: A Case Study in the Spruce-Fir Forest, Quebec, Canada. *Forests*, *6*(2), Article 2. Doi: 10.3390/f6020510.

Gitelson, A.A., Kaufman, Y.J., Merzlyak, M.N., 1996. Use of a green channel in remote sensing of global vegetation from EOS-MODIS. Remote Sens. Environ. 58 (3), 289–298. https://doi.org/10.1016/S0034-4257(96)00072-7.

Gray, D.R., 2008. The relationship between climate and outbreak characteristics of the spruce budworm in eastern Canada. Clim. Change 87 (3), 361–383. https://doi.org/10.1007/s10584-007-9317-5.

Gray, D.R., 2013. The influence of forest composition and climate on outbreak characteristics of the spruce budworm in eastern Canada. Can. J. For. Res. 43 (12), 1181–1195. https://doi.org/10.1139/cjfr-2013-0240.

Gunn, J.S., Ducey, M.J., Buchholz, T., Belair, E.P., 2020. Forest Carbon Resilience of Eastern Spruce Budworm (Choristoneura fumiferana) Salvage Harvesting in the Northeastern United States. Front. For. Global Change 3. https://doi.org/10.3389/ffgc.2020.00014.

Guo, X., Coops, N.C., Tompalski, P., Nielsen, S.E., Bater, C.W., John Stadt, J., 2017. Regional mapping of vegetation structure for biodiversity monitoring using airborne lidar data. Eco. Inform. 38, 50–61. https://doi.org/10.1016/j.ecoinf.2017.01.005.

Hargrove, W.W., Hoffman, F.M., 2004. Potential of Multivariate Quantitative Methods for Delineation and Visualization of Ecoregions. Environ. Manag. 34 (1), S39–S60. https://doi.org/10.1007/s00267-003-1084-0.

Hermosilla, T., Wulder, M.A., White, J.C., Coops, N.C., 2022. Land cover classification in an era of big and open data: Optimizing localized implementation and training data selection to improve mapping outcomes. Remote Sens. Environ. 268, 112780. https://doi.org/10.1016/j.rse.2021.112780.

Hermosilla, T., Wulder, M.A., White, J.C., Coops, N.C., Bater, C.W., Hobart, G.W., 2024. Characterizing long-term tree species dynamics in Canada's forested ecosystems using annual time series remote sensing data. For. Ecol. Manage. 572, 122313. https://doi.org/10.1016/j.foreco.2024.122313.

Hermosilla, T., Wulder, M.A., White, J.C., Coops, N.C., Hobart, G.W., 2015. Regional detection, characterization, and attribution of annual forest change from 1984 to 2012 using Landsat-derived time-series metrics. Remote Sens. Environ. 170, 121–132. https://doi.org/10.1016/j.rse.2015.09.004.

Hermosilla, T., Wulder, M.A., White, J.C., Coops, N.C., Hobart, G.W., Campbell, L.B., 2016. Mass data processing of time series Landsat imagery: Pixels to data products for forest monitoring. Int. J. Digital Earth 9 (11), 1035–1054. https://doi.org/10.1080/17538947.2016.1187673.

Hodgson, D., McDonald, J.L., Hosken, D.J., 2015. What do you mean, 'resilient'? Trends Ecol. Evol. 30 (9), 503–506. https://doi.org/10.1016/j.tree.2015.06.010.

Holling, C.S., 1973. Resilience and Stability of Ecological Systems. Annu. Rev. Ecol. Syst. 4, 1–23.

Holling, C.S., 1996. Engineering Resilience versus Ecological Resilience | Engineering within Ecological Constraints | the National Academies Press. National Academies Press, In Engineering Within Ecological Constraints https://nap.nationalacademies.org/read/4919/chapter/4?term=ecological%20resilience.

Hunt, E.R., Rock, B.N., 1989. Detection of changes in leaf water content using Near- and Middle-Infrared reflectances. Remote Sens. Environ. 30 (1), 43–54. https://doi.org/10.1016/0034-4257(89)90046-1.

Ingrisch, J., Bahn, M., 2018. Towards a Comparable Quantification of Resilience. Trends Ecol. Evol. 33 (4), 251–259. https://doi.org/10.1016/j.tree.2018.01.013.

Johnstone, J.F., Allen, C.D., Franklin, J.F., Frelich, L.E., Harvey, B.J., Higuera, P.E., Mack, M.C., Meentemeyer, R.K., Metz, M.R., Perry, G.L., Schoennagel, T., Turner, M. G., 2016. Changing disturbance regimes, ecological memory, and forest resilience. Front. Ecol. Environ. 14 (7), 369–378. https://doi.org/10.1002/fee.1311.

Jollifee, I.T., 2002. *Principal Component Analysis*. Springer-Verlag. https://doi.org/10.1007/b98835.

Key, C. H., & Benson, N. C. (2006). *Landscape Assessment: Ground measure of severity, the Composite Burn Index; and Remote sensing of severity, the Normalized Burn Ratio* (No. RMRS-GTR-164-CD: LA 1-51). USDA Forest Service, Rocky Mountain Research Station. https://pubs.usgs.gov/publication/2002085.

Kneeshaw, D.D., Sturtevant, B.R., DeGrandpé, L., Doblas-Miranda, E., James, P.M.A., Tardif, D., Burton, P.J., 2021. The Vision of Managing for Pest-Resistant Landscapes: Realistic or Utopic? Curr. For. Rep. 7 (2), 97–113. https://doi.org/10.1007/s40725-021-00140-z.

Lloyd, S., 1982. Least squares quantization in PCM. IEEE Trans. Inf. Theory 28 (2), 129–137. https://doi.org/10.1109/TIT.1982.1056489.

MacLean, D.A., 1980. Vulnerability of Fir-Spruce Stands during Uncontrolled Spruce Budworm Outbreaks: a Review and Discussion. For. Chron. 56 (5), 213–221. https://doi.org/10.5558/tfc56213-5.

MacQueen, J., 1967. Some methods for classification and analysis of multivariate observations. *Proceedings of the Fifth Berkeley Symposium on Mathematical Statistics and Probability*.

Maltman, J.C., Hermosilla, T., Wulder, M.A., Coops, N.C., White, J.C., 2023. Estimating and mapping forest age across Canada's forested ecosystems. Remote Sens. Environ. 290, 113529. https://doi.org/10.1016/j.rse.2023.113529.

Martinez, M., Ardón, M., Gray, J., 2024. Detecting Trajectories of Regime Shifts and loss of Resilience in Coastal Wetlands using Remote Sensing. Ecosystems 27 (8), 1060–1075. https://doi.org/10.1007/s10021-024-00938-5.

Matasci, G., Hermosilla, T., Wulder, M.A., White, J.C., Coops, N.C., Hobart, G.W., Zald, H.S.J., 2018. Large-area mapping of Canadian boreal forest cover, height, biomass and other structural attributes using Landsat composites and lidar plots. Remote Sens. Environ. 209, 90–106. https://doi.org/10.1016/j.rse.2017.12.020.

McNie, P., Kneeshaw, D., Filotas, É., 2023. Landscape-scale patterns of eastern spruce budworm outbreak risk: Defoliation onset vs. tree mortality. Ecosphere 14 (11), e4684.

McNie, P., Kneeshaw, D., Filotas, É., 2024. Increased unpredictability in spruce budworm outbreaks following habitat loss and landscape fragmentation. Ecol. Model. 491, 110675. https://doi.org/10.1016/j.ecolmodel.2024.110675.

Ministère des Ressources Naturelles et des Forêts, 2024a. *Aires infestées par la tordeuse des bourgeons de l'épinette au Québec en 2024*. *1*, 1–34.

Ministère des Ressources Naturelles et des Forêts, 2024b. *Cartographie du cinquième inventaire écoforestier du Québec méridional* (p. 132).

Murtagh, F., Contreras, P., 2012. Algorithms for hierarchical clustering: an overview. WIREs Data Min. Knowl. Discovery 2 (1), 86–97. https://doi.org/10.1002/widm.53.

Navarro, L., Morin, H., Bergeron, Y., Girona, M.M., 2018. Changes in Spatiotemporal patterns of 20th Century Spruce Budworm Outbreaks in Eastern Canadian Boreal Forests. Front. Plant Sci. 9. https://doi.org/10.3389/fpls.2018.01905.

Nealis, V.G., Régnière, J., 2004. Insect-host relationships influencing disturbance by the spruce budworm in a boreal mixedwood forest. Can. J. For. Res. 34 (9), 1870–1882. https://doi.org/10.1139/x04-061.

Nikinmaa, L., de Koning, J.H.C., Derks, J., Grabska-Szwagrzyk, E., Konczal, A.A., Lindner, M., Socha, J., Muys, B., 2024. The priorities in managing forest disturbances to enhance forest resilience: a comparison of a literature analysis and perceptions of forest professionals. Forest Policy Econ. 158, 103119. https://doi.org/10.1016/j.forpol.2023.103119.

Nikinmaa, L., Lindner, M., Cantarello, E., Jump, A.S., Seidl, R., Winkel, G., Muys, B., 2020. Reviewing the use of Resilience Concepts in Forest Sciences. Curr. For. Rep. 6 (2), 61–80. https://doi.org/10.1007/s40725-020-00110-x.

Nimmo, D.G., Mac Nally, R., Cunningham, S.C., Haslem, A., Bennett, A.F., 2015. Vive la résistance: Reviving resistance for 21st century conservation. Trends Ecol. Evol. 30 (9), 516–523. https://doi.org/10.1016/j.tree.2015.07.008.

Pickell, P.D., Hermosilla, T., Frazier, R.J., Coops, N.C., Wulder, M.A., 2016. Forest recovery trends derived from Landsat time series for north American boreal forests. Int. J. Remote Sens. 37 (1), 138–149. https://doi.org/10.1080/2150704X.2015.1126375.

Piene, H., MacLean, D.A., 1999. Spruce budworm defoliation and growth loss in young balsam fir: patterns of shoot, needle and foliage weight production over a nine-year outbreak cycle. For. Ecol. Manage. 123 (2), 115–133. https://doi.org/10.1016/S0378-1127(99)00023-7.

Pothier, D., Elie, J.-G., Auger, I., Mailly, D., Gaudreault, M., 2012. Spruce Budworm-Caused Mortality to Balsam Fir and Black Spruce in Pure and mixed Conifer Stands. For. Sci. 58 (1), 24–33. https://doi.org/10.5849/forsci.10-110.

Power, H., Tremblay, S., Auger, I., Duchateau, E., 2024. Effects of commercial thinning on characteristics of naturally regenerated coniferous stands from Eastern North-America. Can. J. For. Res. 54 (9), 1003–1017. https://doi.org/10.1139/cjfr-2024-0009.

Pureswaran, D.S., Neau, M., Marchand, M., De Grandpré, L., Kneeshaw, D., 2018a. Phenological synchrony between eastern spruce budworm and its host trees increases with warmer temperatures in the boreal forest. Ecol. Evol. 9 (1), 576–586. https://doi.org/10.1002/ece3.4779.

Pureswaran, D.S., Roques, A., Battisti, A., 2018b. Forest Insects and climate Change. Curr. For. Rep. 4 (2), 35–50. https://doi.org/10.1007/s40725-018-0075-6.

Régnière, J., St-Amant, R., Duval, P., 2012. Predicting insect distributions under climate change from physiological responses: Spruce budworm as an example. Biol. Invasions 14 (8), 1571–1586. https://doi.org/10.1007/s10530-010-9918-1.

Rhodes, M.W., Bennie, J.J., Spalding, A., ffrench-Constant, R. H., & Maclean, I. M. D., 2022. Recent advances in the remote sensing of insects. Biol. Rev. 97 (1), 343–360. https://doi.org/10.1111/brv.12802.

Sánchez-Pinillos, M., Leduc, A., Ameztegui, A., Kneeshaw, D., Lloret, F., Coll, L., 2019. Resistance, Resilience or Change: Post-disturbance Dynamics of Boreal Forests after Insect Outbreaks. Ecosystems 22 (8), 1886–1901. https://doi.org/10.1007/s10021-019-00378-6.

Scheffer, M., Carpenter, S.R., Dakos, V., Van Nes, E.H., 2015. Generic indicators of ecological resilience: Inferring the chance of a critical transition. Annu. Rev. Ecol. Evol. Syst. 46 (1), 145–167. https://doi.org/10.1146/annurev-ecolsys-112414-05424.

Scheffer, M., Carpenter, S., Foley, J.A., Folke, C., Walker, B., 2001. Catastrophic shifts in ecosystems. Nature 413 (6856), 591–596. https://doi.org/10.1038/35098000.

Seidl, R., Spies, T.A., Peterson, D.L., Stephens, S.L., Hicke, J.A., 2016. REVIEW: Searching for resilience: addressing the impacts of changing disturbance regimes on forest ecosystem services. J. Appl. Ecol. 53 (1), 120–129. https://doi.org/10.1111/1365-2664.12511.

Senf, C., Seidl, R., Hostert, P., 2017. Remote sensing of forest insect disturbances: current state and future directions. Int. J. Appl. Earth Obs. Geoinf. 60, 49–60. https://doi.org/10.1016/j.jag.2017.04.004.

Šidák, Z., 1967. Rectangular Confidence Regions for the Means of Multivariate Normal Distributions. J. Am. Stat. Assoc. 62 (318), 626–633. https://doi.org/10.2307/2283989.

Smith-Tripp, S.M., Coops, N.C., Mulverhill, C., White, J.C., Axelson, J., 2024. Landsat assessment of variable spectral recovery linked to post-fire forest structure in dry

sub-boreal forests. ISPRS J. Photogramm. Remote Sens. 208, 121–135. https://doi.org/10.1016/j.isprsjprs.2024.01.008.
Snelder, T., Lehmann, A., Lamouroux, N., Leathwick, J., Allenbach, K., 2010. Effect of Classification Procedure on the Performance of Numerically Defined Ecological Regions. Environ. Manag. 45 (5), 939–952. https://doi.org/10.1007/s00267-010-9465-7.
Spence, C.E., MacLean, D.A., 2012. Regeneration and stand development following a spruce budworm outbreak, spruce budworm inspired harvest, and salvage harvest. Can. J. For. Res. 42 (10), 1759–1770. https://doi.org/10.1139/x2012-121.
Standish, R.J., Hobbs, R.J., Mayfield, M.M., Bestelmeyer, B.T., Suding, K.N., Battaglia, L. L., Eviner, V., Hawkes, C.V., Temperton, V.M., Cramer, V.A., Harris, J.A., Funk, J.L., Thomas, P.A., 2014. Resilience in ecology: Abstraction, distraction, or where the action is? Biol. Conserv. 177, 43–51. https://doi.org/10.1016/j.biocon.2014.06.008.
Sturtevant, B.R., Fortin, M.-J., 2021. Understanding and Modeling Forest Disturbance Interactions at the Landscape Level. Front. Ecol. Evol. 9. https://doi.org/10.3389/fevo.2021.653647.
Subedi, A., Marchand, P., Bergeron, Y., Morin, H., Girona, M.M., 2023. Climatic conditions modulate the effect of spruce budworm outbreaks on black spruce growth. Agric. For. Meteorol. 339, 109548. https://doi.org/10.1016/j.agrformet.2023.109548.
Thompson, I.D., Maher, S.C., Rouillard, D.P., Fryxell, J.M., Baker, J.A., 2007. Accuracy of forest inventory mapping: some implications for boreal forest management. For. Ecol. Manage. 252 (1), 208–221. https://doi.org/10.1016/j.foreco.2007.06.033.
Trotto, T., Coops, N.C., Achim, A., Gergel, S.E., Roeser, D., 2024. Characterizing forest structural changes in response to non-stand replacing disturbances using bitemporal airborne laser scanning data. Sci. Remote Sens. 10, 100160. https://doi.org/10.1016/j.srs.2024.100160.
Trotto, T., Coops, N.C., Achim, A., Gergel, S.E., Roeser, D., 2025. Characterizing landscape configuration effects on eastern spruce budworm infestation dynamics. Landsc. Ecol. 40 (9), 183. https://doi.org/10.1007/s10980-025-02203-z.
Trumbore, S., Brando, P., Hartmann, H., 2015. Forest health and global change. Science 349 (6250), 814–818. https://doi.org/10.1126/science.aac6759.
Virgin, G.V.J., MacLean, D.A., 2017. Five decades of balsam fir stand development after spruce budworm-related mortality. For. Ecol. Manage. 400, 129–138. https://doi.org/10.1016/j.foreco.2017.05.057.
Wang, T., Hamann, A., Spittlehouse, D., Carroll, C., 2016. Locally Downscaled and Spatially Customizable climate Data for Historical and Future periods for North America. PLoS One 11 (6), e0156720. https://doi.org/10.1371/journal.pone.0156720.
Ward, J.J.H., 1963. Hierarchical Grouping to Optimize an Objective Function. J. Am. Stat. Assoc. 58 (301), 236–244. https://doi.org/10.1080/01621459.1963.10500845.
White, J.C., Hermosilla, T., Wulder, M.A., Coops, N.C., 2022. Mapping, validating, and interpreting spatio-temporal trends in post-disturbance forest recovery. Remote Sens. Environ. 271, 112904. https://doi.org/10.1016/j.rse.2022.112904.
White, J.C., Wulder, M.A., Hermosilla, T., Coops, N.C., Hobart, G.W., 2017. A nationwide annual characterization of 25 years of forest disturbance and recovery for Canada using Landsat time series. Remote Sens. Environ. 194, 303–321. https://doi.org/10.1016/j.rse.2017.03.035.
White, J.C., Wulder, M.A., Hobart, G.W., Luther, J.E., Hermosilla, T., Griffiths, P., Coops, N.C., Hall, R.J., Hostert, P., Dyk, A., Guindon, L., 2014. Pixel-based image Compositing for Large-Area Dense Time Series applications and Science. Can. J. Remote. Sens. 40 (3), 192–212. https://doi.org/10.1080/07038992.2014.945827.
Woodcock, C.E., Collins, J.B., Gopal, S., Jakabhazy, V.D., Li, X., Macomber, S., Ryherd, S., Judson Harward, V., Levitan, J., Wu, Y., Warbington, R., 1994. Mapping forest vegetation using Landsat TM imagery and a canopy reflectance model. Remote Sens. Environ. 50 (3), 240–254. https://doi.org/10.1016/0034-4257(94)90074-4.
Wulder, M.A., Roy, D.P., Radeloff, V.C., Loveland, T.R., Anderson, M.C., Johnson, D.M., Healey, S., Zhu, Z., Scambos, T.A., Pahlevan, N., Hansen, M., Gorelick, N., Crawford, C.J., Masek, J.G., Hermosilla, T., White, J.C., Belward, A.S., Schaaf, C., Woodcock, C.E., Cook, B.D., 2022. Fifty years of Landsat science and impacts. Remote Sens. Environ. 280, 113195. https://doi.org/10.1016/j.rse.2022.113195.
Wulder, M.A., White, J.C., Nelson, R.F., Næsset, E., Ørka, H.O., Coops, N.C., Hilker, T., Bater, C.W., Gobakken, T., 2012. Lidar sampling for large-area forest characterization: a review. Remote Sens. Environ. 121, 196–209. https://doi.org/10.1016/j.rse.2012.02.001.
Yi, C., Jackson, N., 2021. A review of measuring ecosystem resilience to disturbance. Environ. Res. Lett. 16 (5), 053008. https://doi.org/10.1088/1748-9326/abdf09.
Zhang, B., MacLean, D.A., Johns, R.C., Eveleigh, E.S., 2018. Effects of Hardwood Content on Balsam Fir Defoliation during the Building phase of a Spruce Budworm Outbreak. Forests 9 (9), 9. https://doi.org/10.3390/f9090530.
Zhang, B., MacLean, D.A., Johns, R.C., Eveleigh, E.S., Edwards, S., 2020. Hardwood-softwood composition influences early-instar larval dispersal mortality during a spruce budworm outbreak. For. Ecol. Manage. 463, 118035. https://doi.org/10.1016/j.foreco.2020.118035.